Comprehensive study on ferroelectricity induced by a proper-screw-type magnetic ordering in multiferroic $CuFeO_2$: Nonmagnetic impurity effect on magnetic and ferroelectric order

T. Nakajima,* S. Mitsuda, K. Takahashi, M. Yamano, K. Masuda, and H. Yamazaki
Department of Physics, Faculty of Science, Tokyo University of Science, Tokyo 162-8601, Japan

K. Prokes, K. Kiefer, and S. Gerischer
Helmholtz Centre Berlin for Materials and Energy, Glienicker Straße 100, Berlin 14109, Germany

N. Terada and H. Kitazawa
National Institute for Materials Science, Tsukuba, Ibaraki 305-0044, Japan

M. Matsuda and K. Kakurai
Quantum Beam Science Directorate, Japan Atomic Energy Agency, Tokai, Ibaraki 319-1195, Japan

H. Kimura and Y. Noda
Institute of Multidisciplinary Research for Advanced Materials, Tohoku University, Sendai 980-8577, Japan

M. Soda, M. Matsuura, and K. Hirota
Department of Earth and Space Science, Graduate School of Science, Osaka University, Toyonaka 560-0043, Japan
(Received 31 January 2009; published 16 June 2009)

We refined the magnetic structure of a ferroelectric (FE) phase of multiferroic $CuFe_{1-x}Ga_xO_2$ with $x=0.035$ by complementary use of spherical neutron polarimetry and a four-circle neutron-diffraction measurement, revealing that the proper-screw-type magnetic structure in the ferroelectric phase has a finite ellipticity of ~ 0.9. By means of polarized neutron-diffraction and *in-situ* pyroelectric measurements, we also investigated the quantitative relationship between the macroscopic ferroelectric polarization (P) and the asymmetry in volume fractions with left-handed and right-handed helical magnetic order in $CuFe_{1-x}Al_xO_2$ with $x=0.0155$ and $CuFe_{1-x}Ga_xO_2$ with $x=0.035$. These measurements revealed that the substitution of a small amount of nonmagnetic Ga^{3+} or Al^{3+} ions does not significantly change the magnitude of the local ferroelectric polarization but does reduce the sensitivity of P to the poling electric field (E_p). This implies that the mobility of the magnetic domain walls, which is sensitive to magnetic defects due to nonmagnetic substitution, determines the sensitivity of P to E_p because of a one-to-one correspondence between the magnetic and ferroelectric domains.

DOI: 10.1103/PhysRevB.79.214423 PACS number(s): 75.80.+q, 75.25.+z, 77.80.−e

I. INTRODUCTION

Magnetoelectric (ME) multiferroics, which simultaneously exhibit magnetic and ferroelectric (FE) order, have attracted increasing attention in recent condensed matter physics research because of the interplay they exhibit between ferroelectric and magnetic properties.[1] Among several types of spin-polarization couplings in a variety of ME multiferroics, ferroelectricity induced by a noncollinear magnetic order has been most intensively investigated since Katsura-Nagaosa-Balatsky proposed a robust scheme for magnetically induced electric dipole moment. This was called the "spin-current model,[2]" in which the induced electric dipole moment is given by $\boldsymbol{p} \propto \boldsymbol{e}_{i,i+1} \times (\boldsymbol{S}_i \times \boldsymbol{S}_{i+1})$, where $\boldsymbol{e}_{i,i+1}$ is a unit vector connecting two noncollinear spins, $\boldsymbol{S}_i$ and $\boldsymbol{S}_{i+1}$. This formula successfully explains emergence of ferroelectricity in a variety of noncollinear magnets such as $TbMnO_3$,[3,4] $MnWO_4$,[5,6] and $Ni_3V_2O_8$.[7]

Another type of coupling between ferroelectricity and noncollinear magnetic ordering has been proposed recently; Arima[8] pointed out that variation in *d-p* hybridization with spin-orbit coupling can be a source of ferroelectricity in low-symmetry crystals with noncollinear magnetic order. While the spin current model predicts the ferroelectricity in systems with a "cycloidal" magnetic order, the *d-p* hybridization model predicts the ferroelectricity in materials with a "proper-screw-type" magnetic ordering. A typical example for this model is a delafossite compound $CuFeO_2$ (CFO).

Since the 1990s, CFO has been extensively investigated as a model material of a triangular lattice antiferromagnet, which is a typical example of frustrated spin systems.[9–11] Since the recent discovery of ferroelectricity in the first magnetic-field-induced phase,[12] CFO has attracted increasing interest as a distinct class of ME multiferroics. CFO undergoes a ferroelectric transition at $T_c \sim 10$ K under magnetic fields of $7 \sim 13$ T applied along the hexagonal c axis.[12] Recent studies on $CuFe_{1-x}Al_xO_2$(CFAO) and $CuFe_{1-x}Ga_xO_2$(CFGO) have revealed that the ferroelectric phase is stabilized even in zero magnetic field by substituting a small amount of nonmagnetic Al^{3+} or Ga^{3+} ions for the magnetic Fe^{3+} ions.[13–15] The magnetic structure in the ferroelectric phase is a proper-screw-type, with the propagation wave vector $(q, q, \frac{3}{2})$, where $q \sim 0.21$.[16] Hereafter, we refer to the ferroelectric phase as the ferroelectric incommensurate magnetic (FE-ICM) phase. Recent polarized neutron-diffraction measurements on CFAO($x=0.02$) have demon-

TABLE I. The reported values of the spontaneous electric polarizations in CFO, CFAO, and CFGO at $T=2.0$ K.

Composition	P [$\mu C/m^2$]	E_p [kV/m]	H [T]	Ref.
$CuFeO_2$	~400	~200	12.0	12
$CuFeO_2$	250	~200	12.0	14
$CuFe_{0.99}Al_{0.01}O_2$	250	~200	7.0	14
$CuFe_{0.98}Al_{0.02}O_2$	40	~200	0	14
$CuFe_{0.98}Al_{0.02}O_2$	50	160	0	17
$CuFe_{0.965}Ga_{0.035}O_2$	200	200	0	15

strated that there is a one-to-one correspondence between the spin helicity, left-handed (LH) or right-handed (RH) helical arrangement of spins, and the polarity of the spontaneous electric polarization, which emerges along the helical axis (hexagonal [110] direction).[17] These results suggest that the origin of the ferroelectricity in this system is not explained by the "spin-current" model, but by the *d-p* hybridization model.[8]

One of the unsolved problems regarding the multiferroic property of this system is the magnitude of the macroscopic ferroelectric polarization (P). Table I shows the reported values of P in CFO, CFAO, and CFGO samples. The typical value of P in pure CFO was reported to be 250 ~400 $\mu C/m^2$.[12,14] CFAO($x=0.01$), in which the FE-ICM phase shows up as a magnetic-field-induced state, achieves spontaneous electric polarization of ~250 $\mu C/m^2$.[14] However, CFAO($x=0.02$), in which the FE-ICM phase shows up as a ground state, achieves a rather small P of ~50 $\mu C/m^2$.[14,17] On the other hand, CFGO($x=0.035$) shows a P of ~200 $\mu C/m^2$ even in zero magnetic field.[15] In a previous study, Nakajima *et al.*[16,17] argued that the relatively small P in CFAO($x=0.02$) can be ascribed to the coexistence of the FE-ICM phase and the high-temperature collinear-incommensurate magnetic phase, which is referred to as the partially disordered (PD) phase, at low temperature. However, the fractions of the PD and FE-ICM magnetic orderings have not yet been determined.

In order to completely elucidate the spin-polarization coupling in the CFO system it is critical to answer the following question: "what determines the magnitude of P in this system?" We have thus performed polarized neutron-diffraction and *in-situ* pyroelectric measurements on CFAO and CFGO and also performed pyroelectric measurements on CFO under an applied magnetic field. From these results we have quantitatively determined the nonmagnetic impurity effect on the ferroelectricity in the CFO system.

We have also refined the magnetic structure in the FE-ICM phase. Since CFO (CFAO and CFGO) is a rare example of the ME multiferroics whose ferroelectricity originates from the "proper-screw-type" magnetic ordering, it is critical to determine the magnetic structural parameters in detail, to confirm that the origin of the ferroelectricity is not the "spin-current" model; if the magnetic structure is not the proper-screw-type, but a canted helical (or conical) structure, the emergence of the ferroelectricity can be explained by the spin-current model, as demonstrated in the dielectric measurements on $ZnCr_2Se_4$.[18] In addition, the precise magnetic structural parameters are also indispensable for calculating the volume fractions with the LH and RH helical magnetic orders using the present polarized neutron-diffraction measurements. Therefore, we performed spherical neutron polarimetry and neutron-diffraction measurements with a four-circle diffractometer on a CFGO($x=0.035$) sample.

This paper is organized as follows. In Sec. II we describe experimental details. In Sec. III we present preliminary details of the crystal structure of CFO and the magnetic structure in the FE-ICM phase proposed in the previous study.[16] Sec. IV consists of two subsections. In Sec. IV A we present a detailed refinement of the magnetic structure in the FE-ICM phase with the results of the spherical neutron polarimetry and the neutron-diffraction measurement using a four-circle diffractometer. In Sec. IV B we present the results of the polarized neutron-diffraction and *in situ* pyroelectric measurements on CFAO and CFGO, revealing the quantitative relationship between P and asymmetry in the volume fractions of the RH and LH helical magnetic ordering regions. We also present the poling electric-field dependence of P in pure CFO under applied magnetic field. In Sec. V we summarize our conclusions.

II. EXPERIMENTAL DETAILS

Single crystals of CFO, CFAO($x=0.015$), and CFGO($x=0.035$) of nominal compositions were prepared by the floating zone method.[19]

A. $CuFeO_2$

We performed pyroelectric measurements on pure CFO under applied magnetic fields up to 15 T. The sample was cut into a thin plate ($\sim 3\times 4\times 0.2$ mm^3) with the flat surfaces normal to the hexagonal [110] axis. Silver paste was applied to the large surfaces to form the electrodes. The pyroelectric measurements under applied magnetic fields were carried out using a superconducting cryomagnet installed at National Institute for Materials Science, Tsukuba, Japan. The temperature dependence of P was measured by an electrometer (Keithley 6517A) in a warming run under zero electric field. Before each pyroelectric measurement the sample was cooled from 15 to 2 K under applied magnetic fields and poling electric fields (E_p).

B. $CuFe_{1-x}Al_xO_2$ with $x=0.0155$

Polarized neutron-diffraction and *in situ* pyroelectric measurements on CFAO($x=0.015$) were carried out at the triple-axis neutron spectrometer PONTA installed by the University of Tokyo at JRR-3 in the Japan Atomic Energy Agency (JAEA). An incident-polarized neutron beam with an energy of 34.06 meV was obtained by a Heusler (111) monochromator. The flipping ratio of the polarized neutron beam was ~14. The polarization vector of the incident neutron was set to be parallel or antiparallel to the scattering vector $\boldsymbol{\kappa}(=\boldsymbol{k}_i-\boldsymbol{k}_f)$ by the guide field of a Helmholtz coil and a spin flipper. The collimation was open-40′-40′-80′. A pyrolytic graphite analyzer was employed. The sample was cut into a thin plate

($\sim 3 \times 9 \times 0.8$ mm^3) with the flat surfaces normal to the hexagonal [110] axis and then mounted in a pumped ^{4}He cryostat with an (H,H,L) scattering plane. Silver paste electrodes were applied to the surfaces perpendicular to the [110] axis. The temperature variations in P were deduced by time integration of the observed pyroelectric current, which was measured in a warming run under zero electric field using an electrometer (Keithley 6517A). Before each pyroelectric and neutron-diffraction measurement, the sample was cooled from 20 to 2 K with an applied poling electric field.

C. $CuFe_{1-x}Ga_xO_2$ with $x=0.035$

We performed polarized neutron-diffraction measurements and *in-situ* pyroelectric measurements on CFGO($x=0.035$) at the two-axis neutron diffractometer E4 installed at the Berlin Neutron Scattering Center in the Helmholtz Centre Berlin for Materials and Energy. Spin-polarized incident neutrons with a wavelength of 2.44 Å were obtained by a pyrolytic graphite (002) monochromator and a supermirror polarizer. The flipping ratio of the polarized neutron beam was ~8.3. The polarization vector of the incident neutron was set to be parallel or antiparallel to the scattering vector by the guide field of a Helmholtz coil and a spin flipper. The sample was cut into a thin plate ($\sim 6 \times 10 \times 1$ mm^3) with the widest surfaces normal to the hexagonal [110] axis and then mounted in a pumped ^{4}He cryostat with a hexagonal (H,H,L) scattering plane. Silver paste was applied to the large surfaces of the sample to form the electrodes. The pyroelectric measurements were performed in the same manner as the measurements of CFAO($x=0.015$). To measure the pyroelectric current a Keithley 6514 electrometer was used.

We also refined the magnetic structure in the FE-ICM phase using spherical neutron polarimetry and a four-circle diffractometer for neutron-diffraction measurements. We used a CFGO($x=0.035$) sample with a short cylinder shape (~40 mm^3). Spherical neutron polarimetry was carried out at the triple-axis spectrometer TAS-1 with the CRYOPAD option installed at JRR-3 in JAEA.[20] The energy of spin-polarized incident neutrons was fixed at 14.66 meV. Heusler alloy (111) crystals were used as monochromator and analyzer. The flipping ratio of the polarized neutron beam was ~21. The collimation was open-80′-80′-open. The sample was mounted in a pumped ^{4}He cryostat with a hexagonal (H,H,L) scattering plane. The neutron-diffraction measurements for crystal and magnetic structure analysis were performed using the four-circle neutron diffractometer FONDER installed at JRR-3 in JAEA. An incident neutron beam with wavelength 1.239 Å was obtained using a Ge(311) monochromator. The sample was mounted on a closed-cycle He gas refrigerator.

III. PRELIMINARY DETAILS OF THE SYSTEM

A. Definitions of crystallographic bases

In this paper we have mainly employed the conventional hexagonal basis shown in Fig. 1(a), although CFO originally has a rhombohedral crystal structure. Because of the threefold rotational symmetry along the c axis, the magnetic ordering with the wave vector of $(q,q,\frac{3}{2})$ results in three magnetic domains whose wave vectors of $(q,q,\frac{3}{2})$, $(q,-2q,\frac{3}{2})$, and $(-2q,q,\frac{3}{2})$ are crystallographically equivalent to each other. We refer to the three domains as (110), $(1\bar{2}0)$, and $(\bar{2}10)$, as illustrated in Figs. 1(d)–1(f). In a previous neutron-diffraction study, Terada *et al.*[21] reported that the volume fractions of the three magnetic domains ($V_{(110)}$, $V_{(1\bar{2}0)}$, and $V_{(\bar{2}10)}$) are not equal to each other. The imbalance among the fractions of the three magnetic domains might be ascribed to crystalline defects or the shape of the samples.

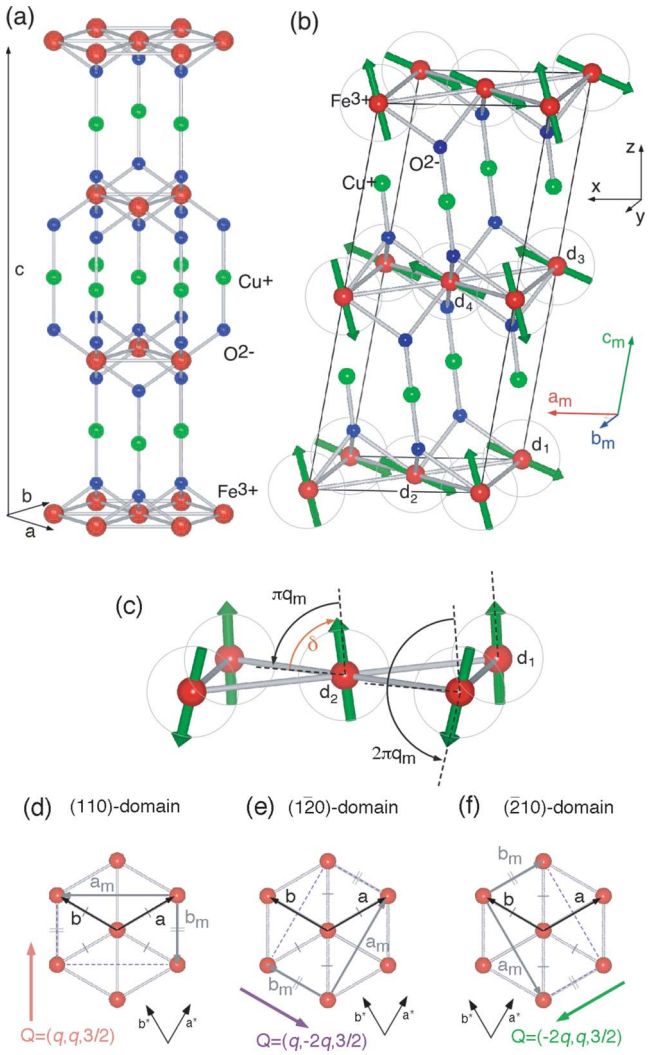

FIG. 1. (Color online) (a) Crystal structure of CFO with the hexagonal basis. (b) The magnetic structure in the FE-ICM phase in $a_m \times b_m \times 2c_m$ cell with monoclinic basis. (c) The definition of the relative phase shift δ. [(d)–(f)] The definition of (d) (110), (e) $(1\bar{2}0)$, and (f) $(\bar{2}10)$ domains and the c projection of the magnetic propagation wave vectors in each domain.

We also employed the monoclinic basis shown in Fig. 1(b). In previous x-ray diffraction measurements, a structural transition from the original trigonal structure to a monoclinic structure has been reported for some of the magnetically ordered phases (including the FE-ICM phase) of CFO (Refs. 22–24) and CFAO.[25] Thus we should employ the monoclinic basis to properly assign the magnetic reflections in the FE-

ICM phase. To distinguish between the two bases, the subscript "m" has been added to the monoclinic notation when referring to modulation wave numbers and reciprocal indices.

B. Magnetic structure in the FE-ICM phase presented in the previous study

The magnetic structure in the FE-ICM phase was determined by the previous neutron-diffraction measurements on CFAO(x=0.012,0.015) under an applied magnetic field.[16] In order to describe the spin components at each Fe^{3+} site, we introduce an $a_m \times b_m \times 2c_m$ cell and a Cartesian coordinate whose x, y, and z axes are parallel to the a_m, b_m, and c axes, as shown in Fig. 1(b). The fractional coordinates of the four Fe^{3+} sites in this cell are given by $\boldsymbol{d}_1=(0,0,0)$, $\boldsymbol{d}_2=(\frac{1}{2},\frac{1}{2},0)$, $\boldsymbol{d}_3=(0,0,1)$, $\boldsymbol{d}_4=(\frac{1}{2},\frac{1}{2},1)$. The spin components at the $\boldsymbol{d}_i$ site are described as follows:

$$S^x_{l,d_i} = \mu_x \cos(\boldsymbol{Q}\cdot(\boldsymbol{l}+\boldsymbol{d}_i)-\phi_i), \tag{1}$$

$$S^y_{l,d_i} = 0, \tag{2}$$

$$S^z_{l,d_i} = \mu_z \sin[\boldsymbol{Q}\cdot(\boldsymbol{l}+\boldsymbol{d}_i)-\phi_i], \tag{3}$$

where μ_x and μ_z are the magnitudes of the magnetic moments along the x and z axes, respectively. $\boldsymbol{Q}$ is the magnetic modulation wave vector, specifically, $\boldsymbol{Q}=(0,q_m,\frac{1}{2})_m[=(q,q,\frac{3}{2})]$. The wave number $q_m(=2q)$ is almost independent of temperature but dependent on applied magnetic field and the concentration of Al^{3+} or Ga^{3+} ions. ϕ_i is the relative phase shift at the $\boldsymbol{d}_i$ site specifically

$$|\phi_1-\phi_2| = |\phi_3-\phi_4| = \delta, \tag{4}$$

$$|\phi_1-\phi_3| = |\phi_2-\phi_4| = 0. \tag{5}$$

In previous experiments, δ was determined to be $\sim 76°$, which corresponds to $\sim \pi q_m$, where $q_m=0.414$ was the wave number of the FE-ICM phase in CFAO(x=0.012,0.0155).[16] μ_x and μ_z were roughly estimated to be $\mu_x=\mu_z \simeq 4\mu_B$.[16] However the previous measurements were not sensitive to the ellipticity of the magnetic structure because of the difficulty in magnetic structure determination by neutron-diffraction measurements under an applied magnetic field.

IV. RESULTS AND DISCUSSION

A. Refinement of magnetic structure in the FE-ICM phase

We refined the magnetic structure in the FE-ICM phase using a CFGO(x=0.035) sample, which exhibits uniform FE-ICM magnetic ordering below $T_c \sim 8.0$ K under zero magnetic field.[15] Since previous measurements have determined a prototypical model of the magnetic structure in the FE-ICM phase,[16] the task remaining for the present study was to refine the magnetic structural parameters in detail. We thus employed two complementary experimental techniques: spherical neutron polarimetry and neutron-diffraction measurements with a four-circle neutron diffractometer.

In principle, all of the magnetic structural parameters in this system can be determined by neutron-diffraction measurements with a four-circle diffractometer. However one might encounter difficulties in the exact determination of ellipticity or spin orientation because of the strong correlation between the parameters; in the magnetic structure determination from the four-circle diffractometer data, the magnetic structural parameters correlate not only with each other but also with the volume fractions of the three magnetic domains. On the other hand, spherical neutron polarimetry can accurately determine the ellipticity and the orientations of the spins but not the absolute values of the magnetic moments, the phase shift δ, or the volume fractions of the three magnetic domains. Therefore we first refined the ellipticity and the orientations of the spins by spherical neutron polarimetry. Subsequently we determined the absolute values of the magnetic moments and δ by neutron-diffraction measurements with the four-circle diffractometer.

1. Spherical neutron polarimetry

In order to define the polarization vector of the incident and scattered neutrons in the present spherical neutron polarimetry we employed another Cartesian coordinate in which the x' axis was parallel to the scattering vector, the z' axis was vertical, and the y' axis completed the right-handed set, as shown in Fig. 2(f). We measured nine different magnetic Bragg reflections belonging to the (110) domain at T =1.4 K [see Fig. 2(e)]. For each reflection we obtained a 3 $\times$3 neutron polarization matrix $P_{\alpha,\beta}$, where α and β denote the polarization directions (x', y', or z') for incident and scattered neutrons, respectively. Among the nine matrix elements, $P_{y',y'}$ and $P_{z',z'}$ are relevant to the ellipticities of the magnetic structures and $P_{y',z'}$ and $P_{z',y'}$ are relevant to the directions of the major and the minor axes of the ellipse drawn by the spin components projected onto the helical plane.

Figures 2(a)–2(d) show the observed values of $P_{y',y'}$, $P_{y',z'}$, $P_{z',y'}$, and $P_{z',z'}$ as functions of ω, which is defined as the angle between the scattering vector for each magnetic reflection and the (110) axis. We found that the values of $P_{y',z'}$ and $P_{z',y'}$ were almost zero for all nine reflections. This indicates that one of the major and minor axes of the ellipse is parallel to the x axis (z' axis); for example, if the minor axis cants from the x axis toward the z axis as shown in Fig. 2(b), the values of $P_{y',z'}$ and $P_{z',y'}$ would be finite around ω=0, as shown in the insets of Figs. 2(b) and 2(c). Taking account of the results mentioned above, we assumed that the magnetic structure is the elliptic helical structure in which the helical axis and the major and minor axes of the ellipse are parallel to the y, z, and x axes, respectively. In this case, $P_{y',y'}$ and $P_{z',z'}$ are described as

$$P_{y',y'} = -P_{z',z'} = \frac{\mu_z^2\cos^2\omega-\mu_x^2}{\mu_z^2\cos^2\omega+\mu_x^2}. \tag{6}$$

We performed a least-square-fitting analysis adapted to Eq. (6). The best fit was obtained for μ_x/μ_z, =0.895(8). Subsequently we refined the directions of the helical axis and the major and minor axes of the ellipse by least-square analysis.

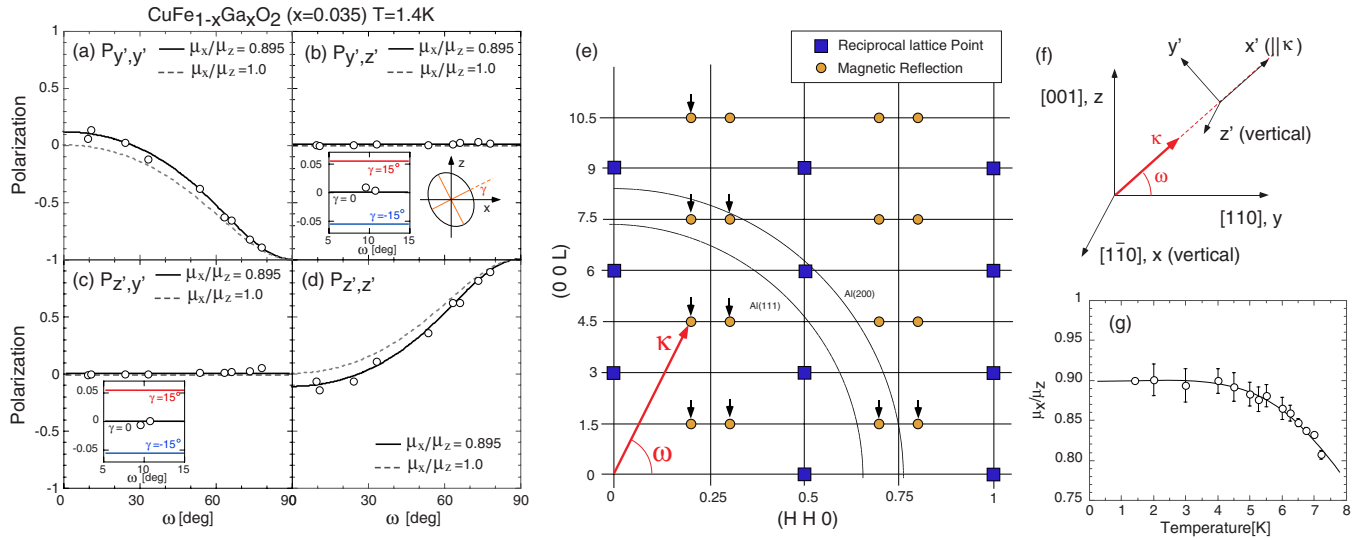

FIG. 2. (Color online) [(a)–(d)] ω dependence of the polarization matrix terms of $P_{y',y'}$, $P_{y',z'}$, $P_{z',y'}$, and $P_{z',z'}$ at $T=1.4$ K. The imperfection of the instrumental beam polarization was corrected by the observed $P_{x',x'}$ term, which should be -1 for a completely polarized neutron beam. The open circles denote the observed values of the polarization matrix terms. The solid and dotted lines denote the calculation for an elliptic helical magnetic structure with $\mu_x/\mu_z=0.895$ and a proper helical magnetic structure ($\mu_x/\mu_z=1.0$), respectively. The insets of (b) and (c) show the magnifications near $\omega=10°$ and the calculations (colored solid lines) for helical magnetic structures whose minor axis cants from the x axis toward the z axis by 15, 0, or $-15°$. (e) A schematic of the (H,H,L) scattering plane and the definition of ω. The black arrows denote the position of the magnetic reflections measured in the present work. (f) The definition of Cartesian coordinates for the magnetic moments at Fe^{3+} sites (x,y,z) and the polarization direction of the incident and scattered neutrons (x',y',z'). (g) Temperature variation in μ_x/μ_z deduced from the results of the present measurement. The solid line is a guide to the eyes.

The analysis showed that the angle γ defined in the inset of Fig. 2(b) was 0 ± 2 degrees and the deviation of the helical axis from the [110] axis was within ~0.6 degrees. From these results we conclude that the magnetic structure in the FE-ICM phase is the elliptic helical magnetic structure, in which the helical axis and the major and minor axes of the ellipse are parallel to the b_m, c, and a_m axes, respectively. This confirms that the origin of the ferroelectricity in this system is not explained by the "spin-current" model, and suggests that the d-p hybridization model is more suitable for explaining the origin of the ferroelectricity.

In order to investigate the temperature dependences of the ellipticities and the directions of the major and minor axes of the ellipse, we measured the polarization matrix terms of the $(q,q,\frac{3}{2})$ and $(\frac{1}{2}-q,\frac{1}{2}-q,\frac{3}{2})$ reflections with increasing temperature. In addition, we also observed the polarization matrix terms of all nine magnetic reflections at $T=6.5$ K. As a result we found that the value of μ_x/μ_z slightly decreased when approaching T_c as shown in Fig. 2(g), while the major and minor axes of the ellipse remained parallel to the c and a_m axes, respectively.

2. Neutron-diffraction measurement with four-circle diffractometer

We performed neutron-diffraction measurements with a four-circle diffractometer in order to determine the absolute values of μ_x, μ_z, and δ. We first performed crystal structure analyses at $T=2.8$ and 6.5 K under zero field to determine the extinction parameter and the scale factor. Integrated intensities of about 50 nuclear Bragg reflections were measured. The procedure of this crystal structure analysis was the same as that used in the previous study on CFAO.[26] As a result, the reliability factors $R(F)$ were 5.10% and 5.40% for $T=2.8$ and 6.5 K, respectively.

For the magnetic structure analysis we measured integrated intensities of more than 130 magnetic Bragg reflections at $T=2.8$ and 6.5 K. The effect of neutron absorption was corrected by the DABEX software. We refined μ_x, μ_z, δ, $V_{(110)}$, $V_{(1\bar{2}0)}$, and $V_{(\bar{2}10)}$, using a homemade least-squares-fitting program in which we set a condition of $V_{(110)}+V_{(1\bar{2}0)}+V_{(\bar{2}10)}=1$ and fixed μ_x/μ_z at the value determined by the present spherical neutron polarimetry. The refined values of μ_x, μ_z, and δ are summarized in Table II. The fractions of the three magnetic domains were determined to be $V_{(110)}:V_{(1\bar{2}0)}:V_{(\bar{2}10)}=0.32:0.29:0.39$ and showed no significant temperature dependence between $T=2.8$ and 6.5 K. A comparison between the observed magnetic structure factor $|F_{obs}|$ and the calculated values $|F_{cal}|$ at $T=2.8$ and 6.5 K are shown in Figs. 3(a) and 3(b). The reliability factors obtained were 6.13% and 7.1% for $T=2.8$ and 6.5 K, respectively.

The relative phase shift δ at $T=2.8$ K was determined to be ~73°, which corresponds to $\sim\pi q_m$ referred to the wave number in the FE-ICM phase of CFGO($x=0.035$), q_m

TABLE II. The results of magnetic structure analysis for CFGO($x=0.035$) at $T=2.8$ and 6.5 K.

T [K]	$\mu_x[\mu_B]$	$\mu_z[\mu_B]$	δ [deg]	$R(F)$ [%]
2.8	3.373 ± 0.006	3.789 ± 0.003	73.4 ± 0.1	6.13
6.5	2.989 ± 0.017	3.472 ± 0.003	69.2 ± 0.1	7.18

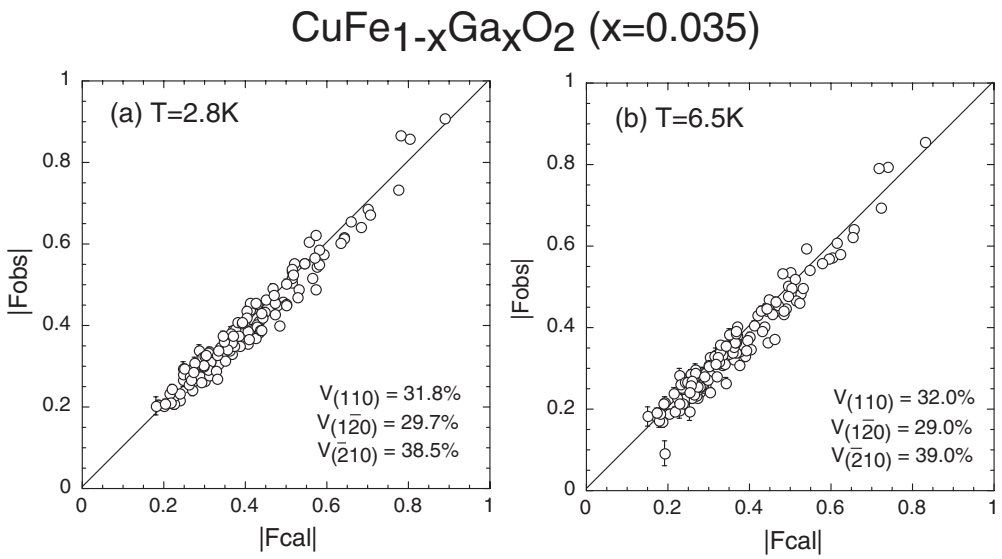

FIG. 3. $|F_{cal}|$ vs $|F_{obs}|$ plots obtained from the magnetic structure analysis for CFGO(x=0.035) at (a) T=2.8 K and (b) T=6.5 K.

=0.406. This indicates that the spin at $\boldsymbol{d}_2$ site is arranged to be parallel to the spin at the $\boldsymbol{d}_1$ site, in other words, the spins at $\boldsymbol{d}_1$ and $\boldsymbol{d}_2$ sites are ferromagnetically arranged. This is consistent with the results of the previous magnetic structure analysis.[16] However, the present results revealed that δ slightly degreased with increasing temperature, while q was independent of temperature in the FE-ICM phase.[15]

Note that we also tried to determine all of the magnetic structural parameters from only the four-circle diffractometer data. In this analysis, the ellipticity was determined to be ~0.9 and the angle between the x axis and the minor axis of the ellipse γ was determined to be ~15°. Although this value of γ did not agree with the results of the spherical neutron polarimetry, we ascribed the disagreement to the strong correlation between the parameters and the imperfect corrections for the absorption and extinction effects. Therefore, in the present analysis, we fixed the ellipticity (μ_x/μ_z) and directions of the helical axis and the minor and major axes of the ellipse to values determined from the spherical neutron polarimetry.

B. Poling electric field dependence of electric polarization and asymmetry in spin helicity

In the previous polarized neutron-diffraction study on CFAO(x=0.02), Nakajima *et al.*[17] revealed that there is a one-to-one correspondence between the spin helicity and the polarity of the induced ferroelectric polarization. Therefore, in the present study we performed polarized neutron-diffraction and *in-situ* pyroelectric measurements on CFGO(x=0.035) and CFAO(x=0.015) and deduced the magnitude of the local ferroelectric polarization from the E_p dependences of P and the asymmetry in the volume fractions with the RH and LH helical magnetic order. This enabled us to quantitatively investigate the nonmagnetic impurity effect on the ferroelectricity in the CFO system.

Before discussing the present results, we briefly review the scattering cross-sections for polarized neutrons. In the present measurements we mainly measured two magnetic Bragg reflections of $(q,q,\frac{3}{2})$ and $(\frac{1}{2}-q,\frac{1}{2}-q,\frac{3}{2})$. These reflections were assigned as $\boldsymbol{\tau}+\boldsymbol{Q}$ and $\boldsymbol{\tau}-\boldsymbol{Q}$ reflections using the monoclinic basis in the (110) domain, where $\boldsymbol{\tau}$ is a reciprocal lattice vector. The scattering cross-section for these reflections is given by[27,28]

$$\left(\frac{d\sigma}{d\Omega}\right)_{\boldsymbol{\tau}\pm\boldsymbol{Q}} \propto S(\boldsymbol{\kappa})\{(\mu_{x\perp}^2+\mu_{z\perp}^2)[V_{(110)}^{\mathrm{RH}}+V_{(110)}^{\mathrm{LH}}] \mp 2\mu_{x\perp}\mu_{z\perp}(\boldsymbol{p}_{\mathrm{N}}\cdot\hat{\boldsymbol{\kappa}})[V_{(110)}^{\mathrm{RH}}-V_{(110)}^{\mathrm{LH}}]\}, \quad (7)$$

where $S(\boldsymbol{\kappa})$ is a factor dependent on the magnetic form factor and δ. $\mu_{x\perp}$ and $\mu_{z\perp}$ are the lengths of the spin components projected onto the plane normal to the scattering vector. $V_{(110)}^{\mathrm{RH}}$ and $V_{(110)}^{\mathrm{LH}}$ are the volume fractions having RH and LH helical magnetic order in the (110) domains, respectively. $\hat{\boldsymbol{\kappa}}$ and $\boldsymbol{p}_N$ are unit vectors of the scattering vector and the polarization direction of the incident neutrons, respectively.

In this paper we refer to the asymmetry of $V_{(110)}^{\mathrm{RH}}$ and $V_{(110)}^{\mathrm{LH}}$ as $D_{(110)}(E_p)$. From Eq. (7) $D_{(110)}(E_p)$ is given by

$$D_{(110)}(E_p)=\frac{V_{(110)}^{\mathrm{LH}}-V_{(110)}^{\mathrm{RH}}}{V_{(110)}^{\mathrm{LH}}+V_{(110)}^{\mathrm{RH}}}=A(\boldsymbol{\kappa})\left(\frac{I_{\mathrm{ON}}-I_{\mathrm{OFF}}}{I_{\mathrm{ON}}+I_{\mathrm{OFF}}}\right)p_0^{-1}, \quad (8)$$

where p_0 is the instrumental beam polarization of the incident neutrons. I_{ON} and I_{OFF} are the intensities of a magnetic Bragg reflection measured when the spin flipper is on ($\boldsymbol{p}_N\|\boldsymbol{\kappa}$) and off ($\boldsymbol{p}_N\|-\boldsymbol{\kappa}$), respectively. From the results of the present magnetic structure refinement, the proportional constant $A(\boldsymbol{\kappa})$ for the $(q,q,\frac{3}{2})$ and $(\frac{1}{2}-q,\frac{1}{2}-q,\frac{3}{2})$ reflections were calculated to be 1.002 and −1.004, respectively.

We define the directions of "positive" and "negative" poling electric fields as the [110] and [$\bar{1}\bar{1}$0] directions, respectively. Note that these two directions are crystallographically distinguishable because of the trigonal symmetry of the crystal [see Fig. 4(b)].

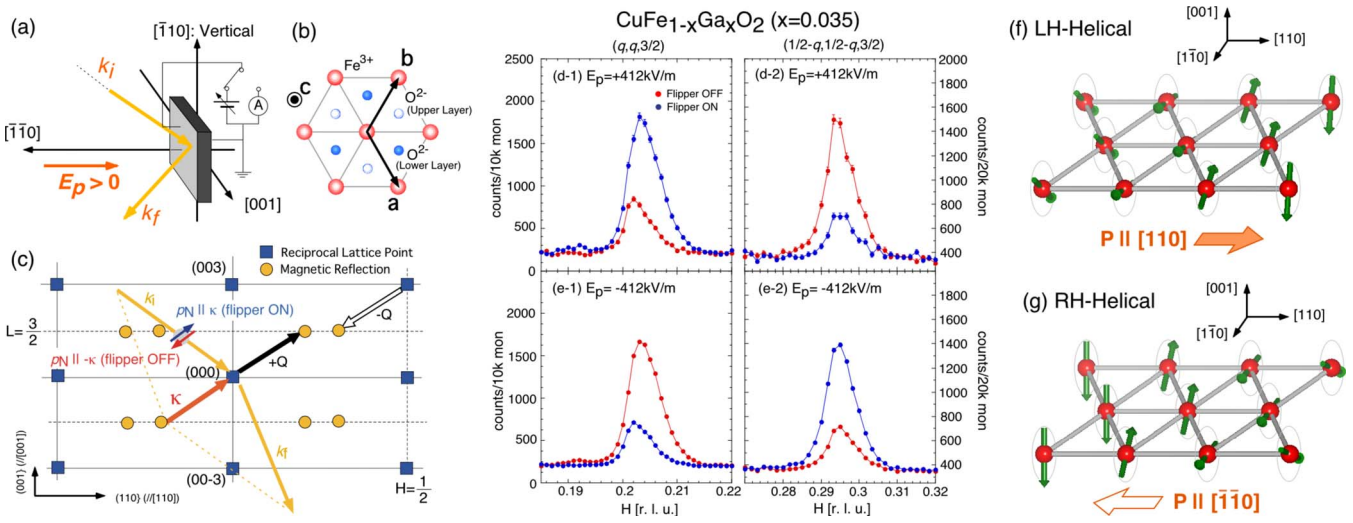

FIG. 4. (Color online) (a) The schematic of the present experimental setup and the definition of the "positive" poling electric field. (b) The definition of the hexagonal basis in the crystal structure of CFO. The [110] direction differs in the positions of O^{2-} ions from the $[\bar{1}\bar{1}0]$ direction. (c) The schematic of the reciprocal lattice map of CFGO and the directions of the polarization vector of the incident neutrons. (d) and (e) The diffraction profiles of $(H,H,\frac{3}{2})$, reciprocal lattice scans for the $(q,q,\frac{3}{2})$, and $(\frac{1}{2}-q,\frac{1}{2}-q,\frac{3}{2})$ magnetic Bragg reflections at $T=2.0$ K in the FE-ICM phase. [(f)–(g)] The relationship between the spin helicity and the direction of the induced ferroelectric polarization.

1. $CuFe_{1-x}Ga_xO_2$ *with* $x=0.035$

Figures 4(d) and 4(e) show typical diffraction profiles of CFGO(x=0.035) at T=2.0 K after cooling under applied poling electric fields (E_p) of ±412 kV/m. When the sample was cooled under a positive poling electric field, I_{ON} was greater than I_{OFF} for the $(q,q,\frac{3}{2})$ reflection, and this relationship between I_{ON} and I_{OFF} was reversed for the $(\frac{1}{2}-q,\frac{1}{2}-q,\frac{3}{2})$ reflection, as shown in Fig. 4(d). By a reversal of the sign of E_p, this relationship between I_{ON} and I_{OFF} for each magnetic satellite was also reversed, as shown in Fig. 4(e). These results indicate that the LH and RH helical magnetic orderings generate a spontaneous electric polarization parallel to the [110] and $[\bar{1}\bar{1}0]$ directions, respectively [see Figs. 4(f) and 4(g)]. This relationship is consistent with the results of the previous polarized neutron-diffraction measurements on CFAO(x=0.02).[17,28]

We now focus on the relationship between P and $D_{(110)}(E_p)$. In the present study we measured the E_p dependences of P and $D_{(110)}(E_p)$ by the following procedure: before each measurement, the sample was cooled from 20 to 2 K under the poling electric field of E_p. At T=2 K, the poling electric field was removed and the electrode terminal of the sample was kept shorted for about 300 s to reduce the residual current. We first performed the polarized neutron-diffraction measurement at 2 K to obtain $D_{(110)}(E)$. Subsequently we performed the pyroelectric measurement in a warming run to obtain P at 2 K.

Figure 5(a) shows the E_p dependence of $D_{(110)}(E_p)$ at T=2.0 K. In the electric field region of $|E_p|<\sim 200$ kV/m, $D_{(110)}(E_p)$ rapidly increased with increasing E_p. However, $D_{(110)}(E_p)$ tended to be insensitive to E_p in the region of $|E_p|>\sim 200$ kV/m. On the other hand, no significant E_p dependence was found in the sum of I_{ON} and I_{OFF}, which corresponds to $V_{LH}^{(110)}+V_{RH}^{(110)}(=V_{(110)})$, as shown in Fig. 5(b). This indicates that the ratio among $V_{(110)}$, $V_{(1\bar{2}0)}$, and $V_{(\bar{2}10)}$ did not depend on E_p.

Figure 5(c) shows the E_p dependence of P at T=2.0 K. Although P exhibited a similar E_p dependence to $D_{(110)}(E_p)$, P was not exactly proportional to $D_{(110)}(E_p)$ in the present experimental settings. This is because the ferroelectric polar-

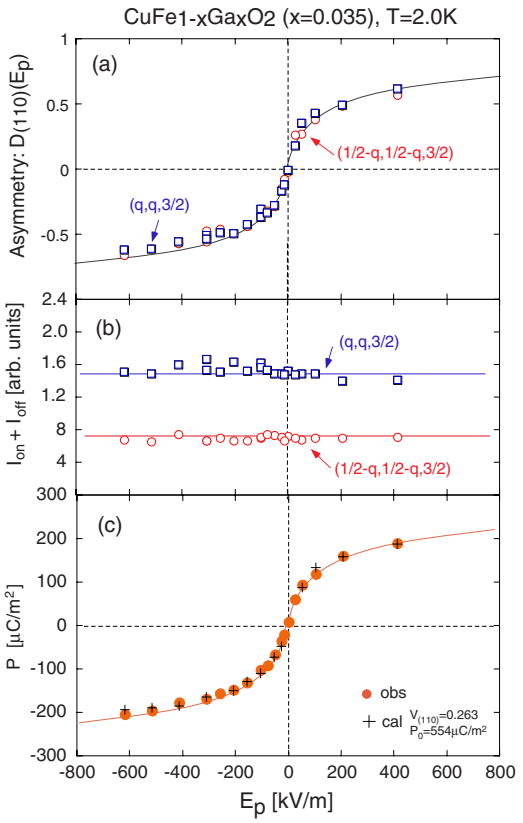

FIG. 5. (Color online) The E_p dependences of (a)$D_{(110)}(E_p)$ in the (110) domain, (b) the sum of $I_{ON}+I_{OFF}$, and (c) the observed and calculated values of P in CFGO(x=0.035) at T=2.0 K. The solid lines are guides to the eyes, drawn so as to be symmetric.

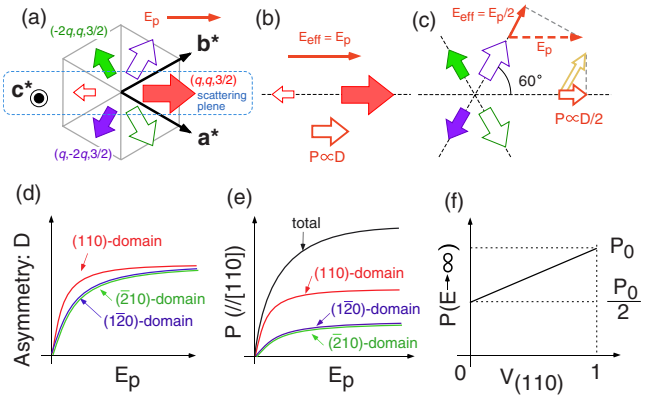

FIG. 6. (Color online) (a) A schematic of the distribution of the RH (open arrows) and LH (filled arrows) helical magnetic orderings in the (110), $(1\bar{2}0)$, and $(\bar{2}10)$ domains when the macroscopic P emerges along the [110] axis. The size of the arrows shows the fractions of the LH (or RH) helical magnetic ordering. (b) The relationship between the direction of E_p and the local ferroelectric polarization in (110) domain, and (c) that in $(1\bar{2}0)$ and $(\bar{2}10)$ domains. E_{eff} is the projection of E_p onto the direction of the ferroelectric polarization in each domain. (d) and (e) The schematic drawing of E_p dependence of (d) $D_{(110)}(E_p)$ and (e) electric polarization projected on the [110] axis in each magnetic domain. (f) $V_{(110)}$ dependence of P in the case of $D_{(110)}=D_{(1\bar{2}0)}=D_{(\bar{2}10)}=1$.

ization in the $(1\bar{2}0)$ and $(\bar{2}10)$ domains contributed to the observed macroscopic ferroelectric polarization along the [110] axis. In order to estimate the contributions, we should determine the asymmetries in the volume fractions with the LH and RH helical magnetic order within the $(1\bar{2}0)$ and $(\bar{2}10)$ domains and the ratio among $V_{(110)}$, $V_{(1\bar{2}0)}$, and $V_{(\bar{2}10)}$. However, in the present polarized neutron-diffraction measurements in the (H,H,L) scattering plane, we cannot directly determine these values.

In order to overcome this problem we focused on the curvatures of the E_p dependence of P and $D_{(110)}(E_p)$. As illustrated in Figs. 6(b) and 6(c), the projection of the poling electric field on the directions of the ferroelectric polarization in the $(\bar{2}10)$ [or $(1\bar{2}0)$] domain was half of that in the (110) domain. We thus assume the following equation

$$|D_{(\bar{2}10)}(E_p)| = |D_{(1\bar{2}0)}(E_p)| = |D_{(110)}(E_p/2)|. \tag{9}$$

In addition, in the $(1\bar{2}0)$ [or $(\bar{2}10)$] domain, the [110] projection of the ferroelectric polarization was also half the magnitude of the ferroelectric polarization vector, as depicted in Fig. 6(c). Therefore, the macroscopic electric polarization along [110] axis is described as

$$P(E_p) = P_0 V_{(110)} D_{(110)}(E_p) + \frac{P_0}{2}(1 - V_{(110)}) D_{(110)}(E_p/2), \tag{10}$$

where P_0 is the value of P for a single-domain state, that is, $V_{(110)}:V_{(1\bar{2}0)}:V_{(\bar{2}10)}=1:0:0$ and $D_{(110)}=1$. In Figs. 6(d) and 6(e) we show schematic of the E_p dependences of the ferroelectric polarization projected along the [110] axis and the asymmetry in the volume fractions of RH and LH helical magnetic order in each domain.

It should be emphasized that P_0 is a truly fundamental value to evaluate the magnitude of the local ferroelectric polarization in this system, while a saturation value of P observed in a pyroelectric measurement must be dependent on the ratio of the three magnetic domains originating from the trigonal symmetry of the crystal. For example, if $V_{(1\bar{2}0)}$ [or $V_{(\bar{2}10)}$] is dominant, the projection of the electric polarization on the [110] axis should be reduced, compared with the case when $V_{(110)}$ is dominant [see Fig. 6(f)].

Note that we cannot use the value of $V_{(110)}$ determined in Sec. IV A for Eq. (10) because we used two different crystals for the magnetic structure analysis and the polarized neutron-diffraction and *in-situ* pyroelectric measurements. Although the compositions of these samples were the same, the magnetic domain distributions might have differed.

We refined P_0 and $V_{(110)}$ using a least-squares-fitting program adopted to Eq. (10) with the observed values of $D_{(110)}(E_p)$. The best fit was obtained for $P_0=554$ $\mu\text{C}/\text{m}^2$ and $V_{(110)}=0.263$. The comparison between the observed and calculated P is shown in Fig. 5(c).

2. $CuFe_{1-x}Al_xO_2$ *with* $x=0.015$

We performed polarized neutron-diffraction and *in-situ* pyroelectric measurements on CFAO($x=0.015$) in the same manner as we performed on CFGO($x=0.035$). Figures 7(a) and 7(b) show typical diffraction profiles at $T=2.0$ K, measured after the cooling process under positive and negative poling electric fields. The relationship between I_{ON} and I_{OFF} at each reflection was the same as in CFGO($x=0.035$). This shows that the one-to-one correspondence between the polarity of P and the spin helicity in the magnetic ordering is common to CFAO and CFGO.

Before discussing the E_p dependence of $D_{(110)}(E_p)$ in CFAO($x=0.0155$), we should determine the fraction of the PD magnetic ordering, which was considered to coexist with the FE-ICM phase under zero magnetic field. In the previous study, Terada *et al.*[21] pointed out that the neutron-diffraction profile in the zero field FE-ICM phase in CFAO($x=0.0155$) is characterized by the two wave numbers, $q_1 \sim 0.207$ and $q_2 \sim 0.213$. Actually, in the present measurement, a diffusive magnetic reflection with the wave number of $q_2 \sim 0.213$ was observed in the shoulder of the main peak with the wave number of $q_1 \sim 0.207$, as shown in Fig. 7(a). Since the reflection at q_2 was not observed in the magnetic-field-induced FE-ICM phase in CFAO($x=0.012$), Nakajima *et al.*[16] ascribed the magnetic reflection around q_2 to the coexistence of high-temperature PD magnetic ordering, whose magnetic structure is a collinear-incommensurate structure with a wave number of $q_{\text{PD}} \sim 0.213$.

The fraction of collinear magnetic ordering can be determined by polarized neutron-diffraction measurements. The intensity of a magnetic Bragg reflection from a collinear magnetic structure does not depend on the polarization direction of the incident neutron, while that from a helical magnetic structure it does. Therefore, in Fig. 7(c), we compare the profiles of $I_{\text{ON}}-I_{\text{OFF}}$ and $I_{\text{ON}}+I_{\text{OFF}}$; the former is proportional to the magnetic reflection only from the helical mag-

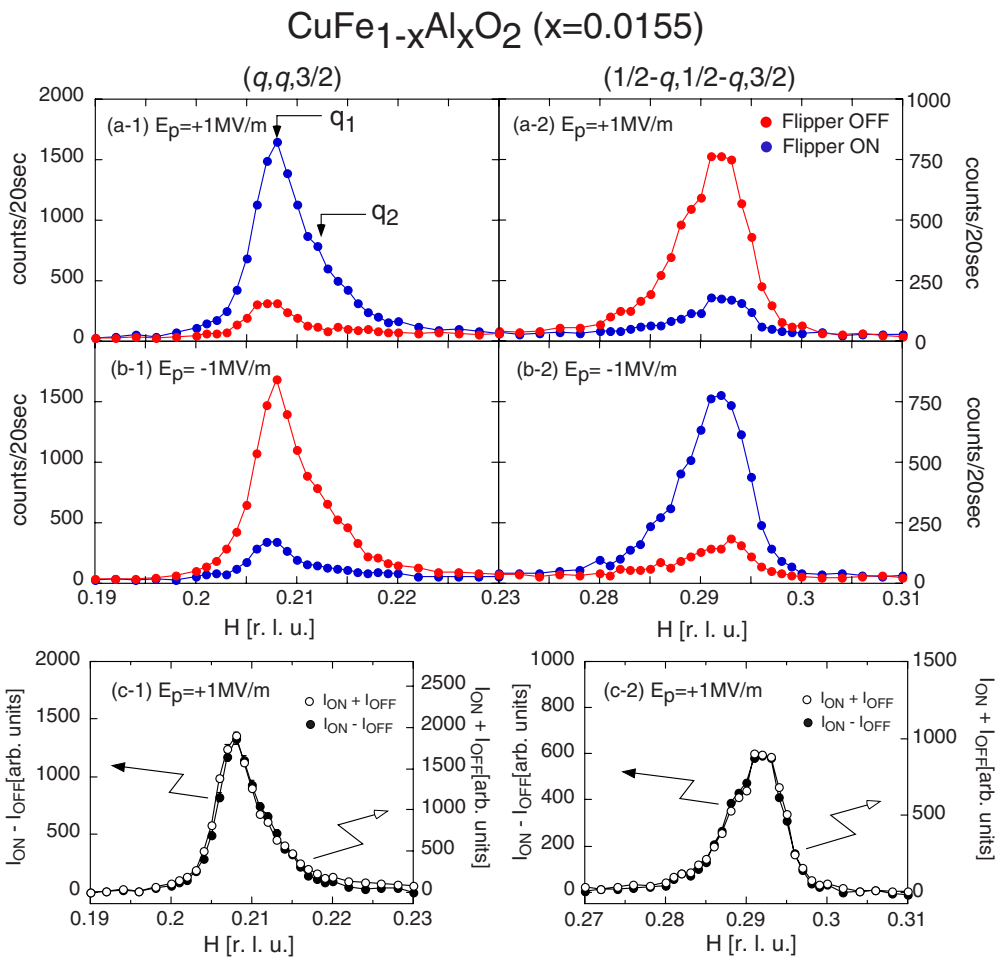

FIG. 7. (Color online) (a) and (b) Diffraction profiles of $(H,H,\frac{3}{2})$, reciprocal lattice scans for the $(q,q,\frac{3}{2})$, and $(\frac{1}{2}-q,\frac{1}{2}-q,\frac{3}{2})$ magnetic Bragg reflections at $T=2.0$ K in the FE-ICM phase of CFAO($x=0.015$). (c) A comparison between the profiles of $I_{\mathrm{ON}}-I_{\mathrm{OFF}}$ (open circles) and $I_{\mathrm{ON}}+I_{\mathrm{OFF}}$ (filled circles) for the $(q,q,\frac{3}{2})$ and $(\frac{1}{2}-q,\frac{1}{2}-q,\frac{3}{2})$ magnetic Bragg reflections at $T=2.0$ K.

netic orderings, while the later is proportional to the total magnetic reflections. As a result, we found that the profiles of $I_{\mathrm{ON}}-I_{\mathrm{OFF}}$ and $I_{\mathrm{ON}}+I_{\mathrm{OFF}}$ were almost the same within the experimental accuracy. This implies that both of the magnetic reflections at q_1 and q_2 correspond to the helical magnetic ordering, that is, the ground state of CFAO($x=0.015$) is almost a "single" FE-ICM phase.

In order to confirm the single FE-ICM state in CFAO($x=0.015$), we performed a temperature scan under an applied electric field of 1 MV/m. At $T=8.14$ K, in the PD phase, there was no helical magnetic ordering, as shown in Fig. 8(a). At $T=7.63$ K, just below T_c, the magnetic reflection from the helical magnetic ordering was observed to emerge around $q_2\sim 0.213$, which is the almost the same wave number as q_{PD}. With decreasing temperature, the magnetic reflection from the helical magnetic ordering with wave number $q_1\sim 0.207$ started to grow below $T\sim 6.8$ K, as shown in Fig. 8(c). Below $T\sim 5$ K, the magnetic reflection from the PD magnetic ordering almost disappeared and the magnetic reflections from the FE-ICM magnetic orderings with the wave numbers q_1 and q_2 coexisted. Figure 8(e) also shows that the diffraction profiles in the "single" FE-ICM phase in CFAO($x=0.015$) are rather broad, compared with the experimental resolution. These results can be interpreted as follows: the local magnetic structure in the ground state of CFAO($x=0.015$) is helical magnetic ordering. However, the system does not exhibit a true long-range ordered state, but consists of relatively small domains, in which the propagation wave numbers in each domain are slightly different from each other. The difference in the modulation wave number in each domain might be caused by macroscopic inhomogeneity of the nonmagnetic impurities.

We now focus on the E_p dependences of P and $D_{(110)}(E_p)$ in CFAO($x=0.015$). As shown in Figs. 9(a)–9(c), the values of P and $D_{(110)}(E_p)$ monotonically increased with increasing E_p, while no significant E_p dependence was found in $I_{\mathrm{ON}}+I_{\mathrm{OFF}}$. These results are almost the same as the results of CFGO($x=0.035$). However, we found that P and $D_{(110)}(E_p)$ in CFAO($x=0.015$) were rather insensitive to E_p, compared with those in CFGO($x=0.035$).

We refined P_0 and $V_{(110)}$ by least-squares analysis in the same manner as in the analysis of CFGO. The comparison between the calculated and observed values of P is shown in Fig. 9(c). The best fit was obtained for $P_0=456$ $\mu\mathrm{C/m^2}$ and $V_{(110)}=0.28$. This result shows that CFAO can achieve a ferroelectric polarization comparable to the typical values of P in pure CFO.

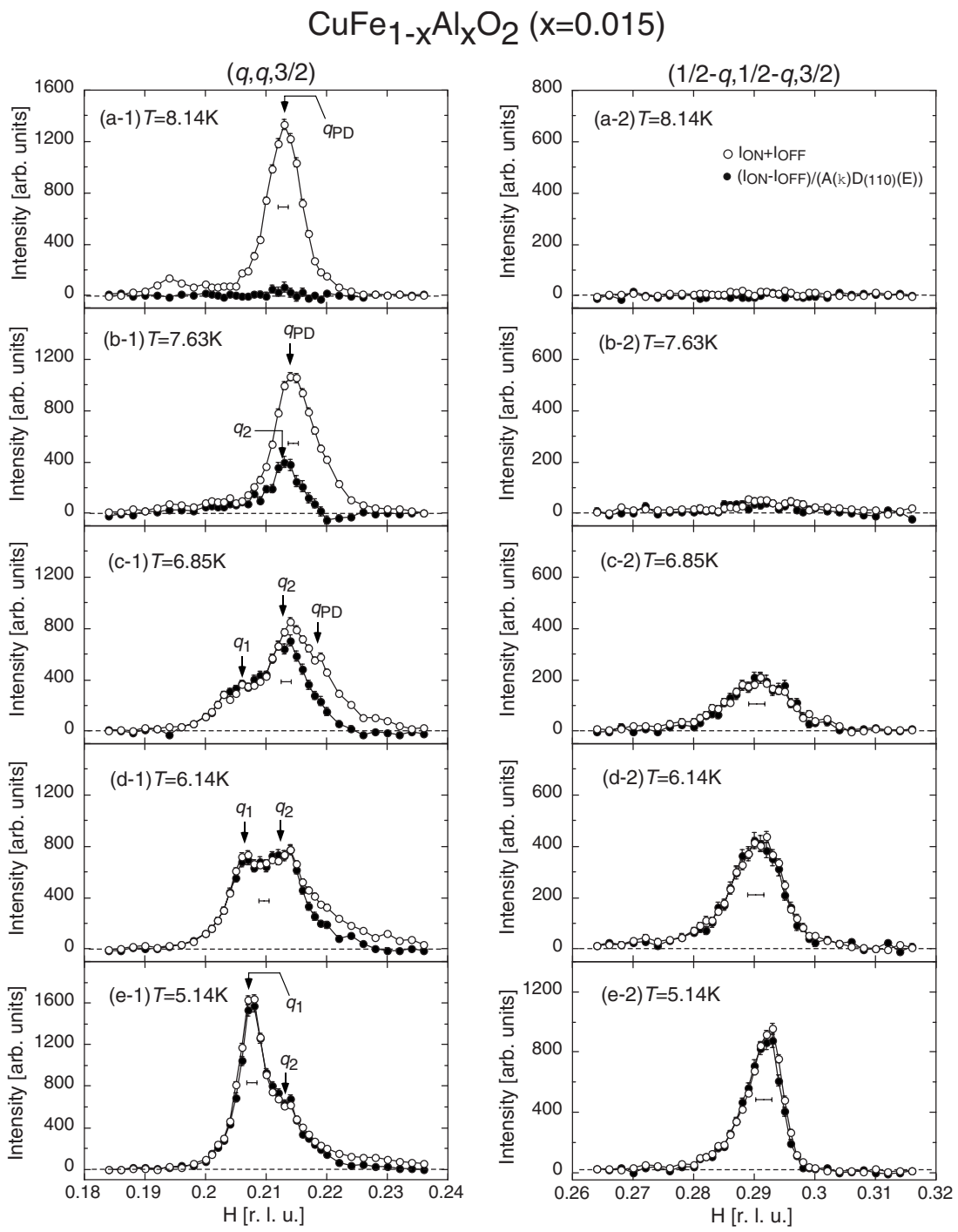

FIG. 8. Temperature variations in the diffraction profiles of $(q,q,\frac{3}{2})_h$ and $(\frac{1}{2}-q,\frac{1}{2}-q,\frac{3}{2})$ magnetic Bragg reflections in the cooling process with E_p of +1 MV/m. The open and filled symbols denote the diffraction intensities from the sum of the collinear and helical magnetic orderings ($I_{ON}+I_{OFF}$) and the reflection only from the helical magnetic ordering ($I_{ON}-I_{OFF}$), respectively. The data of $I_{ON}-I_{OFF}$ were multiplied by $A(\kappa)^{-1}D_{(110)}(E_p)^{-1}$, where $D_{(110)}(E_p)^{-1}$ was deduced from the intensities for $(\frac{1}{2}-q,\frac{1}{2}-q,\frac{3}{2})$ reflections at $T=5.14$ K in order to directly compare with $I_{ON}+I_{OFF}$. The horizontal bars represent the experimental resolution.

3. $CuFeO_2$

In order to estimate the value of P_0 in pure CFO, we performed pyroelectric measurements under an applied magnetic field along the c axis up to 15 T. Figure 10 shows the temperature variations in P measured after cooling under several E_p at $H=12$ T, where the wave number of the FE-ICM magnetic ordering $q\sim0.202$ was close to that in CFGO($x=0.035$).[10,15] The E_p dependence of P at $T=2.0$ K is shown in the inset. From these results, the maximum value of P was roughly estimated to be ~420 $\mu C/m^2$. Because of the difficulty of making polarized neutron-diffraction measurements under applied magnetic field, we cannot determine

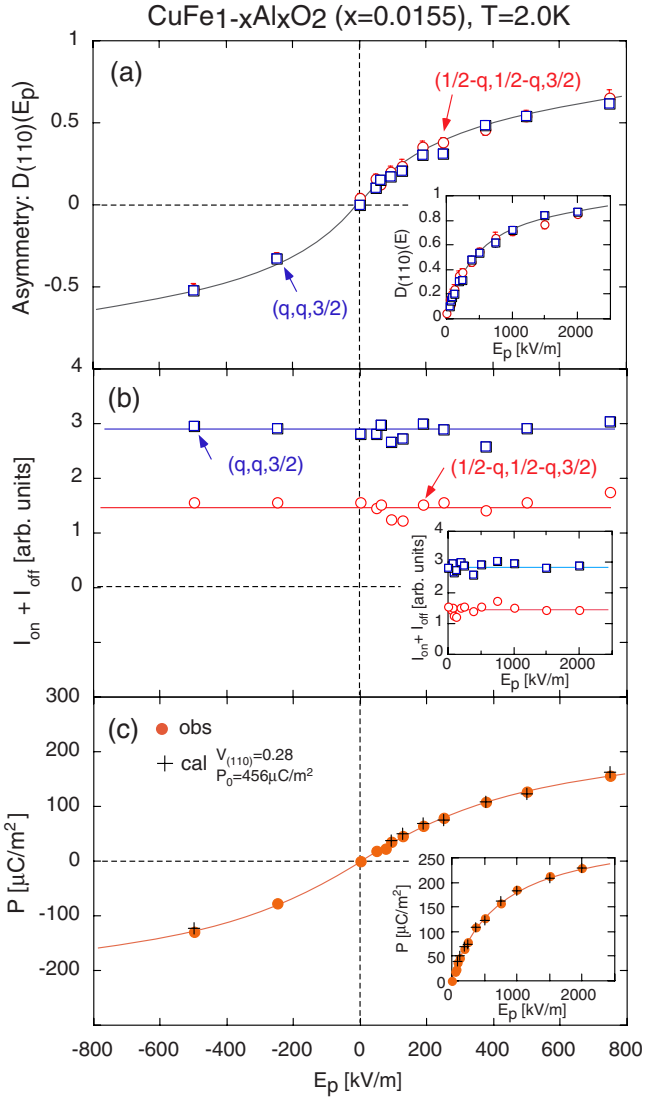

FIG. 9. (Color online) The E_p dependences of (a) $D_{(110)}(E_p)$ in the (110) domain, (b) the sum of $I_{ON}+I_{OFF}$, and (c) the observed and calculated values of P in CFAO(x=0.015) at T=2.0 K. The solid lines are guides to the eyes, drawn so as to be symmetric.

$D_{(110)}(E_p)$ and $V_{(110)}$ in the FE-ICM phase of pure CFO. Assuming that $V_{(110)}=1/3$ and $D_{(110)}(E_p\rightarrow\infty)=1.0$, we can roughly estimate P_0 in CFO under an applied magnetic field of 12 T to be $\sim 630\ \mu C/m^2$.

4. Summary of E_p dependence of P and $D_{(110)}$

We performed polarized neutron-diffraction and *in-situ* pyroelectric measurements on CFGO(x=0.035) and CFAO(x=0.015) and also performed pyroelectric measurements on CFO under applied magnetic fields in order to answer the question, "what determines the magnitude of P in this system?" As mentioned in introduction, the previously reported values of P in CFO,[12,14] CFAO,[14,17] and CFGO (Ref. 15) are rather different from each other (these values span the range from 40 to 400 $\mu C/m^2$). These previous results imply that nonmagnetic substitution affects the magnitude of the local ferroelectric polarization and/or the E_p dependence of the asymmetry in the RH and LH helical magnetic orderings.

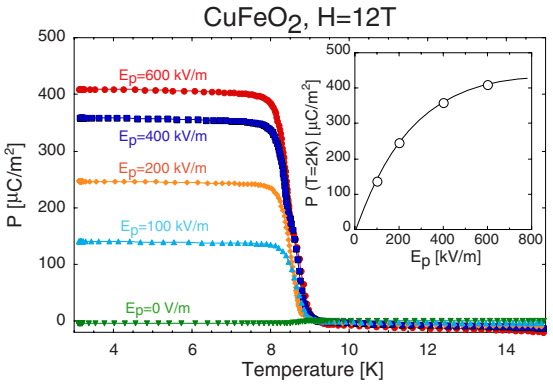

FIG. 10. (Color online) Temperature variations in P under an applied magnetic field of 12 T along the c axis measured after cooling processes with several E_p. The inset shows the E_p dependence of P at T=2.0 K and H=12 T. The solid line is a guide to the eyes.

In the present study we revealed that the values of P_0 in CFO, CFAO, and CFGO are comparable to each other, as summarized in Table III. This indicates that the substitution of a small amount of nonmagnetic Al^{3+} or Ga^{3+} ions does not largely reduce the magnitude of the local ferroelectric polarization in the CFO system. We also revealed that nonmagnetic substitution affects the E_p dependence of $D_{(110)}(E_p)$. In particular, Al substitution more remarkably reduces the sensitivity of $D_{(110)}(E_p)$ to E_p than Ga substitution, as summarized in Fig. 11. This must be the reason for the large difference in the previously reported values of P, which were measured with the relatively low E_p of $\sim$200 kV/m.

One of the most obvious differences between the FE-ICM magnetic orderings in CFAO and CFGO is the neutron-diffraction profiles, which suggest that CFGO(x=0.035) exhibits a relatively homogeneous FE-ICM magnetic state, while CFAO(x=0.015) has an inhomogeneous domain state. Therefore we conclude that the imperfection of the long-range magnetic ordering in the FE-ICM phase is relevant to the reduction in the sensitivity of $D_{(110)}(E_p)$ to E_p, and results in the reduction in the sensitivity of P to E_p.

For the microscopic mechanism of the reduction in the sensitivity of P to E_p, it is reasonable to propose the following scenario: at the ferroelectric transition, where the system undergoes a first-order magnetic phase transition from the PD phase to the FE-ICM phase, the poling electric field

TABLE III. The values of P_0 in CFO, CFAO, and CFGO obtained in the present study. Since $D_{(110)}(E_p)$ in pure CFO was not determined by the present measurements, the value of P_0 for CFO is a mere estimation (see the main text for the details).

Composition	P_0 [$\mu C/m^2$]	T [K]	H [T]	q [r.l.u]
$CuFeO_2$	$\sim$630	2.0	12.0	0.202
$CuFe_{0.985}Al_{0.015}O_2$	456 ± 37	2.0	0	$\sim$0.21
$CuFe_{0.965}Ga_{0.035}O_2$	554 ± 24	2.0	0	0.203

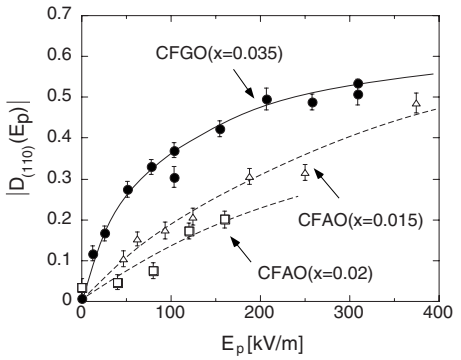

FIG. 11. The E_p dependences of $D_{(110)}(E_p)$ in CFGO(x =0.035), CFAO(x=0.015), and CFAO(x=0.02) (taken from Ref. 17) at T=2 K. The solid and dashed lines are guides to the eyes.

populates either of the RH or LH helical magnetic domains so that the macroscopic electric polarization is parallel to it. However, the magnetic defects due to the nonmagnetic substitution reduce the mobility of the magnetic domain walls. Consequently, the sensitivity of P to E_p is reduced because of the one-to-one correspondence between the magnetic and ferroelectric domains. In particular, Al substitution affects the mobility of the magnetic domain walls more strongly than Ga substitution. This is because the substitution of Al^{3+} ions introduces not only magnetic vacancies but also local lattice distortions due to the large difference in the ionic radii of Al^{3+} and Fe^{3+} ions. These local lattice distortions randomly lift the local degeneracy in the competing exchange interactions and strongly disturb the coherent magnetic ordering, as pointed out by Terada *et al.*[15] As a result, in CFAO, the mobility of the magnetic domain walls is significantly reduced and therefore the sensitivity of P to E_p is largely reduced.

Finally we discuss the q dependence of P_0 in this system. In Ref. 8, Arima pointed out that the magnitude of the ferroelectric polarization in the *d-p* hybridization model must depend on the modulation wave number q. Actually, the magnetic field dependences of P and q in pure CFO suggest a correlation between them.[10,12] However, the detailed magnetic structural parameters under magnetic fields beyond ~7 T, where CFO exhibits the FE-ICM phase, have not yet been determined. Therefore, a comparison between the values of P_0 in CFAO(x=0.015) and CFGO(x=0.035) is a good test for checking the applicability of the *d-p* hybridization model. In Table III we summarize P_0 and q in CFAO(x =0.015) and CFGO(x=0.035). Here we estimated the average of q in CFAO(x=0.015) to be ~0.21. By using Eq. (3) in Ref. 25, $P_0(q=0.210)/P_0(q=0.203)$ was calculated to be ~0.91. This ratio is consistent with the observed ratio of P_0[CFAO(x=0.015)]/P_0[CFGO(x=0.035)]~0.82±0.07, suggesting that the *d-p* hybridization model successfully reproduces the observed q dependence of P_0.

V. CONCLUSION

We refined the magnetic structure in the FE-ICM phase of multiferroic CFGO(x=0.035) by a complementary use of spherical neutron polarimetry and neutron-diffraction measurement with a four-circle diffractometer. As a result, we revealed that the magnetic structure in the FE-ICM phase is the elliptic helical magnetic structure in which the helical axis and the major and minor axes of the ellipse are parallel to the b_m, c, and a_m axes, respectively. The ellipticity was determined to be ~0.9. These results confirm that the origin of the ferroelectricity in CFO systems is not explained by the "spin-current" model, and suggest the *d-p* hybridization model[8] is more suitable for explaining the origin of the ferroelectricity.

We also quantitatively investigated the relationship between P and the asymmetry in the volume fractions with LH and RH helical magnetic order in CFAO(x=0.015) and CFGO(x=0.035) by means of polarized neutron-diffraction and *in-situ* pyroelectric measurements. Although the previously reported values of P in CFO, CFAO, and CFGO are rather different from each other as mentioned in introduction, the present results revealed that the substitution of a small amount of nonmagnetic Ga^{3+} or Al^{3+} ions does not affect the magnitude of the local ferroelectric polarization but affects the E_p dependence of the asymmetry in the fractions with RH and LH helical magnetic order. Consequently, nonmagnetic substitution reduces the sensitivity of P to E_p. These results suggest that the mobility of the magnetic domain walls, which is sensitive to the existence of magnetic defects due to the nonmagnetic substitution, determines the E_p dependence of P because of the one-to-one correspondence between the magnetic and ferroelectric domains. The present results imply the possibility that nonmagnetic impurities, which reduce the mobility of magnetic domain walls, can be used as a tool for tuning the sensitivity of ME responses in a variety of multiferroics.

ACKNOWLEDGMENTS

The neutron-diffraction measurements at JRR-3 were carried out along the proposals No. 8541B and No. 8779 and partly supported by ISSP of the University of Tokyo. The neutron-diffraction measurement at BENSC was carried out along the proposal No. PHY-01-2126. We thank D. Draht for technical help with the preparation of the experiment at Helmholtz Centre Berlin. This work was supported by a Grant-in-Aid for Scientific Research (C) (Grant No. 19540377), a Grant-in-Aid for Young Scientist (B) (Grant No. 20740209), and a Grant-in-Aid for Scientific Research in Priority Area "Novel States of Matter Induced by Frustration" (Grants No. 19052001, No. 19052002, No. 19052004, and No. 19052008), from JSPS, Japan. The images of the crystal and magnetic structures in this paper were depicted using the software VESTA (Ref. 29) developed by K. Monma.

*nakajima@nsmsmac4.ph.kagu.tus.ac.jp

[1] T. Kimura, T. Goto, H. Shintani, K. Ishizaka, T. Arima, and Y. Tokura, Nature (London) **426**, 55 (2003).
[2] H. Katsura, N. Nagaosa, and A. V. Balatsky, Phys. Rev. Lett. **95**, 057205 (2005).
[3] M. Kenzelmann, A. B. Harris, S. Jonas, C. Broholm, J. Schefer, S. B. Kim, C. L. Zhang, S.-W. Cheong, O. P. Vajk, and J. W. Lynn, Phys. Rev. Lett. **95**, 087206 (2005).
[4] Y. Yamasaki, H. Sagayama, T. Goto, M. Matsuura, K. Hirota, T. Arima, and Y. Tokura, Phys. Rev. Lett. **98**, 147204 (2007).
[5] K. Taniguchi, N. Abe, T. Takenobu, Y. Iwasa, and T. Arima, Phys. Rev. Lett. **97**, 097203 (2006).
[6] H. Sagayama, K. Taniguchi, N. Abe, T. H. Arima, M. Soda, M. Matsuura, and K. Hirota, Phys. Rev. B **77**, 220407(R) (2008).
[7] G. Lawes, A. B. Harris, T. Kimura, N. Rogado, R. J. Cava, A. Aharony, O. Entin-Wohlman, T. Yildrim, M. Kenzelmann, C. Broholm, and A. P. Ramirez, Phys. Rev. Lett. **95**, 087205 (2005).
[8] T. Arima, J. Phys. Soc. Jpn. **76**, 073702 (2007).
[9] S. Mitsuda, H. Yoshizawa, N. Yaguchi, and M. Mekata, J. Phys. Soc. Jpn. **60**, 1885 (1991).
[10] S. Mitsuda, M. Mase, K. Prokes, H. Kitazawa, and H. A. Katori, J. Phys. Soc. Jpn. **69**, 3513 (2000).
[11] O. A. Petrenko, M. R. Lees, G. Balakrishnan, S. de Brion, and G. Chouteau, J. Phys.: Condens. Matter **17**, 2741 (2005).
[12] T. Kimura, J. C. Lashley, and A. P. Ramirez, Phys. Rev. B **73**, 220401(R) (2006).
[13] S. Kanetsuki, S. Mitsuda, T. Nakajima, D. Anazawa, H. A. Katori, and K. Prokes, J. Phys.: Condens. Matter **19**, 145244 (2007).
[14] S. Seki, Y. Yamasaki, Y. Shiomi, S. Iguchi, Y. Onose, and Y. Tokura, Phys. Rev. B **75**, 100403(R) (2007).
[15] N. Terada, T. Nakajima, S. Mitsuda, H. Kitazawa, K. Kaneko, and N. Metoki, Phys. Rev. B **78**, 014101 (2008).
[16] T. Nakajima, S. Mitsuda, S. Kanetsuki, K. Prokes, A. Podlesnyak, H. Kimura, and Y. Noda, J. Phys. Soc. Jpn. **76**, 043709 (2007).
[17] T. Nakajima, S. Mitsuda, S. Kanetsuki, K. Tanaka, K. Fujii, N. Terada, M. Soda, M. Matsuura, and K. Hirota, Phys. Rev. B **77**, 052401 (2008).
[18] H. Murakawa, Y. Onose, K. Ohgushi, S. Ishiwata, and Y. Tokura, J. Phys. Soc. Jpn. **77**, 043709 (2008).
[19] T. R. Zhao, M. Hasegawa, and H. Takei, J. Cryst. Growth **166**, 408 (1996).
[20] M. Takeda, M. Nakamura, K. Kakurai, E. Lelièvre-Berna, F. Tasset, and L.-P. Regnault, Physica B **356**, 136 (2005).
[21] N. Terada, S. Mitsuda, T. Fujii, K. Soejima, I. Doi, H. A. Katori, and Y. Noda, J. Phys. Soc. Jpn. **74**, 2604 (2005).
[22] N. Terada, S. Mitsuda, H. Ohsumi, and K. Tajima, J. Phys. Soc. Jpn. **75**, 023602 (2006).
[23] N. Terada, Y. Tanaka, Y. Tabata, K. Katsumata, A. Kikkawa, and S. Mitsuda, J. Phys. Soc. Jpn. **75**, 113702 (2006).
[24] F. Ye, Y. Ren, Q. Huang, J. A. Fernandez-Baca, Pengcheng Dai, J. W. Lynn, and T. Kimura, Phys. Rev. B **73**, 220404(R) (2006).
[25] T. Nakajima, S. Mitsuda, T. Inami, N. Terada, H. Ohsumi, K. Prokes, and A. Podlesnyak, Phys. Rev. B **78**, 024106 (2008).
[26] N. Terada, T. Kawasaki, S. Mitsuda, H. Kimura, and Y. Noda, J. Phys. Soc. Jpn. **74**, 1561 (2005).
[27] M. Blume, Phys. Rev. **130**, 1670 (1963).
[28] The relationship between the spin helicity and the polarity of P in CFAO(x=0.02) presented in Ref. 17 is incorrect, because of the misapplication of the formula of the scattering cross-section in Ref. 27 to the previous experimental setup. The relationship among the direction of $\boldsymbol{p}_N$, the neutron-diffraction intensities and the direction of the poling electric field in the present study is the same as that in the previous study on CFAO(x=0.02) in Ref. 17. This indicates that the one-to-one correspondence between the spin helicity and the polarity of P shown in Figs. 4(f) and 4(g) in this paper is common to CFAO(x=0.02), CFAO(x=0.015), and CFGO(x=0.035).
[29] K. Momma and F. Izumi, J. Appl. Crystallogr. **41**, 653 (2008).